Si Radial *p-i-n* Junction Photovoltaic Arrays with Built-In Light Concentrators

Jinkyoung Yoo,*,† Binh-Minh Nguyen,†,∥ Ian H. Campbell,‡ Shadi A. Dayeh,§ Paul Schuele,⊥ David Evans,⊥ and S. Tom Picraux*,†

†Center for Integrated Nanotechnologies, Los Alamos National Laboratory, Los Alamos, New Mexico 87545, United States, ‡Materials Physics and Applications—11, Los Alamos National Laboratory, Los Alamos, New Mexico 87545, United States, §Department of Electrical and Computer Engineering, University of California San Diego, La Jolla, California 92093, United States, and ⊥Sharp Laboratories, Camas, Washington 98607, United States. ∥Present address: HRL Laboratories, Malibu, California 90265, United States.

ABSTRACT High-performance photovoltaic (PV) devices require strong light absorption, low reflection and efficient photogenerated carrier collection for high quantum efficiency. Previous optical studies of vertical wires arrays have revealed that extremely efficient light absorption in the visible wavelengths is achievable. Photovoltaic studies have further advanced the wire approach by employing radial *p-n* junction architectures to achieve more efficient carrier collection. While radial *p-n* junction formation and optimized light absorption have independently been considered, PV efficiencies have further opportunities for enhancement by exploiting the radial *p-n* junction fabrication procedures to form arrays that simultaneously enhance *both* light absorption and carrier collection efficiency. Here we report a concept of morphology control to improve PV performance, light absorption and quantum efficiency of silicon radial *p-i-n* junction arrays. Surface energy minimization during vapor phase epitaxy is exploited to form match-head structures at the tips of the wires. The match-head structure acts as a built-in light concentrator and enhances optical absorptance and external quantum efficiencies by 30 to 40%, and PV efficiency under AM 1.5G illumination by 20% compared to cylindrical structures without match-heads. The design rules for these improvements with match-head arrays are systematically studied. This approach of process-enhanced control of three-dimensional Si morphologies provides a fab-compatible way to enhance the PV performance of Si radial *p-n* junction wire arrays.

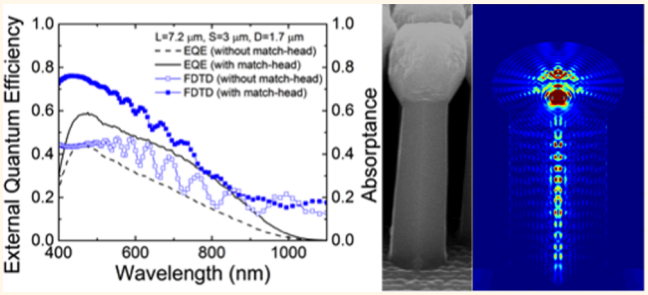

KEYWORDS: photovoltaic · radial *p-n* junction · silicon nanowire · quantum efficiency · finite difference time domain calculation

Lowering the levelized cost of energy by obtaining higher photogenerated electric power, while maintaining low fabrication and operation costs, is the golden rule in photovoltaic (PV) cell research. Conventional approaches to obtaining higher photogenerated electric power in PV devices include the enhancement of light absorption, the use of multiple junctions, or the use of light concentrators. From the perspective of enhanced light absorption, the nanostructuring of solar absorber materials is one of the promising approaches being pursued, since the small size provides pathways for both reducing reflection and enhancing light absorption.[1] The development of design rules to maximize light absorption has been a focus of studies to enhance PV performance for nanowire (NW) arrays. The main approach used in these studies has been to employ optical absorption spectroscopy in combination with simulations by finite domain time difference (FDTD) or rigorous couple-wave analysis (RCWA) methods.[2−5] These studies of the optical properties of NWs have shown excellent light absorption behavior over the solar spectrum, with a focus on optimizing NW sizes, shapes, and geometrical arrangements to maximize array light absorption.[6−10] However, in spite of these advances in enhancing optical absorption, progress is still needed in enhancing the PV efficiency of Si NW cells (currently 10−18.2%),[11−15] suggesting that attention is needed on simultaneously enhancing light absorption and carrier collection efficiency through NW design.

* Address correspondence to jyoo@lanl.gov, picraux@lanl.gov.

Received for review January 23, 2015 and accepted May 11, 2015.

Published online May 11, 2015
10.1021/acsnano.5b00500

Radial *p-n* junction wire architectures have been considered as building blocks for high-performance NW PV devices since the architecture offers a novel opportunity to maximize light absorption while enhancing photogenerated carrier collection efficiency.[16,17] In principle, the maximum PV conversion efficiency for a radial *p-n* junction structure can be obtained in cases of a wire diameter comparable to the minority-carrier diffusion length.[16] Thus, Si wires with diameters ranging from 1 to 10 μm are of particular interest for PV studies according to recent studies of minority-carrier diffusion lengths of Si nano/microwires.[18,19] Engineering the Si wire PV architecture *via* control of the wire shape provides an additional degree of freedom for designing PV cells. For example, radial shell growth can lead to changes in the wire shape from symmetric cylinders to faceted surfaces, which can influence the optical absorption properties.[5,11,20] In addition, previous studies[11,20] have shown that the facets formed during radial epitaxy on wires can result in match-head-like structures, similar to lens-like structures on planar PV cells.[21] These match-heads on wire PV structures offer a new architecture for controlling optoelectronic properties.

Combined studies of both optical absorption and carrier collection provides valuable insights into ways to use such wire structural designs to enhance PV device performance. Experimentally, the external quantum efficiency (EQE), the ratio of the number of collected carriers to the number of incident photons, as a function of incident wavelength provides a valuable determination of the combined optical absorption and photogenerated carrier collection for a PV architecture. Comparing the wavelength-dependent EQE and simulated optical absorption provides an excellent method to better understand the interplay between optical absorption and material structuring in governing the carrier collection efficiency. Thus, a detailed analysis of the physical factors affecting EQE and the resulting PV efficiency for a new architecture offers new understanding for performance improvements in Si radial *p-n* junction wire array solar cells.

Here we report the enhancement in PV performance for a new architecture, Si radial *p-i-n* junction wire arrays with match-heads at their tips, and carry out a systematic study of the measured EQE and simulated optical absorption as a function of incident wavelength for Si radial *p-i-n* junction arrays with match-head structures at the tip of the wires. Using epitaxial growth of Si radial *p-i-n* shells we demonstrate a significant enhancement in light absorption and EQE for Si radial junction arrays with match-head structures compared to cylindrical Si radial *p-i-n* junction arrays without match-heads. While previous optical absorption studies have demonstrated the benefits of tapered wire structures for enhancing light absorption,[2,4,13] no prior work to our knowledge has fabricated or discussed the benefits of such larger match-head sizes at the wire tips. The advantage of match-head structures on both EQE and PV performance of Si radial *p-i-n* junction arrays is presented in this article. Additionally by comparing the measured EQE values of Si radial *p-i-n* junction arrays with the finite difference time domain (FDTD) simulations, we demonstrate the optimization of wire lengths, diameters and filling factors, and show that carrier collection at small diameters becomes a more important consideration than maximizing optical absorption for optimized PV efficiency.

RESULTS AND DISCUSSION

Electron Microscopy and Current–Voltage Characteristics. The epitaxial growth of the radial *p-i-n* junctions depends on the presence of dopants[22] in a way that enables one to tailor the structure and morphology of the wire arrays. This knowledge can in turn be used to further optimize their PV performance. One fascinating aspect of this epitaxial growth evolution is the formation of match-head like structures at the wire tips. This effect is due to the increased Si surface adatom diffusion in the presence of boron (B) dopants, which induces a lower surface step energy on the Si surfaces and gives in a multifaceted minimal surface energy structure with {110} and {311} planes resulting in a match-head shape at the end of the wires.[11,23] In contrast, the phosphorus (P) doped Si radial growth hinders Si adatom migration and induces a drastic lowering of the Si shell growth rate,[24] thus suppressing the multifacet formation and match-head growth.[11]

In this study, Si radial *p-i-n* junction array devices with and without match heads are prepared as shown in Figure 1(a). The core Si wire etching and the electrode formation were carried out in the same processing batches to ensure the only difference between the two devices is the existence of the match-head, with all other process variables kept identical. For the Si radial *p-i-n* junction array without match-heads, 1.3 μm-diameter core *p*-type Si wires were fabricated and then 100 nm-thick intrinsic (*i*) Si and 100 nm-thick *n*-type Si(P) radial shells were grown. For the Si radial *p-i-n* junction array with match-heads, 0.7 μm-diameter core *p*-type Si wires were prepared, followed by the growth of 300 nm-thick *p*-type Si(B), 100 nm-thick *i*-Si, and 100 nm-thick *n*-type Si(P) radial shells. By starting with the smaller wire radius for the match-head case and using a similar *p*-type doping level for both the *p*-type Si substrate and the Si(B) epitaxial growth layer, the radial doping profiles and final wire diameter for both the match-head wires and the nonmatch-head wires are kept approximately the same. The match-head is thus be expected to have a *p*-type core covered by the same *i* and *n*-shells as along the length of the NWs. As seen from Figure 1(a) and (b), for the present case a 300 nm-thick Si(B) radial shell growth induces a clear match-head formation with 2 μm diameter match-heads at the tip of

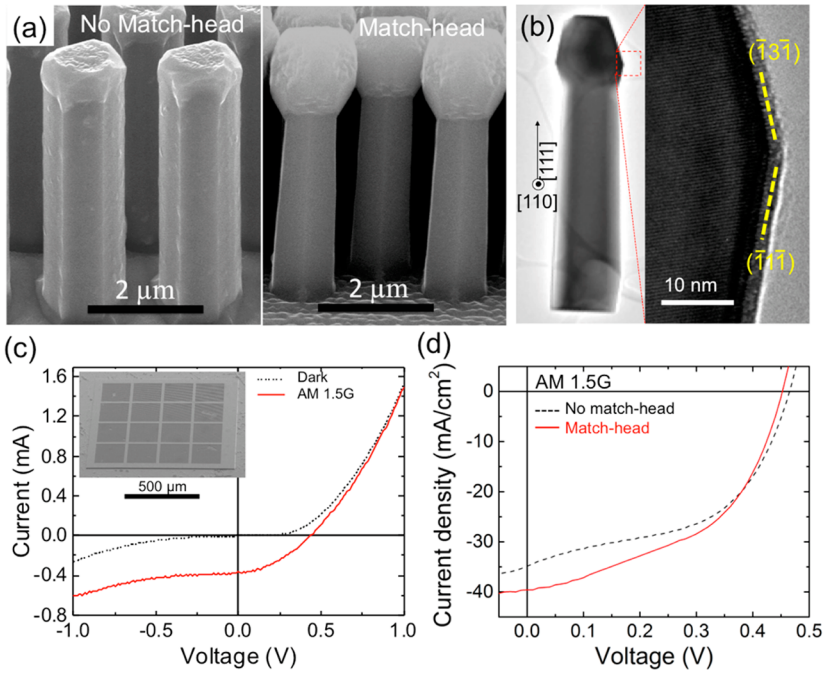

Figure 1. (a) The scanning electron microscopy (SEM) image of Si radial *p-i-n* junction wire arrays with and without match-heads. The match-head morphology was obtained by epitaxial *p*-type Si radial shell growth *via* chemical vapor deposition growth on core *p*-type Si NWs with the fixed thicknesses of intrinsic and n-type Si shells of 100 nm (see text for details of how the same *p-i-n* junction profiles are obtained). (b) The transmission electron microscopy images of a single Si wire after growth of a 100 nm-thick *p*-type Si(B) radial shell. The low magnification image (left) shows facets at the top of the wire, and the high-resolution image (right) displays the single crystalline facets consisting of {113} and {111} planes. (c) The current–voltage (*I*–*V*) characteristic curve of a Si radial *p-i-n* junction array under dark (dashed line) and AM 1.5G illumination condition (solid line). The metal top electrodes were fabricated on the surfaces just outside the wire arrays. The inset is the tilted-view low magnification SEM image of 1 × 1 mm^2-Si radial *p-i-n* junction arrays with match-heads. (d) The current density–voltage characteristic curves of a Si radial *p-i-n* junction arrays with (red, solid) and without (black, dashed) match-heads under AM 1.5G illumination condition. The diameter of stems and the lengths are 1.3 and 7 μm, respectively, in both Si radial *p-i-n* junction arrays. The PV efficiencies of Si radial *p-i-n* junction arrays without and with match-head structures for these devices were 8.2 and 10.1%, respectively.

the 1.7-μm diameter wires. Detailed examination of the surface structure of the match-head by transmission electron microscopy reveals {110} and {311} surface facets as shown in Figure 1(b). After the radial epitaxy growth steps, metal electrodes on *n*-type and *p*-type regions were formed on adjacent planar pads (Figure S1 in the Supporting Information). Each electrode and associated Si radial *p-i-n* junction wire array were isolated from other arrays by mesa fabrication. The details of the device fabrication scheme are described in the Supporting Information.

Evaluation of PV Response of Si Match-Head Radial P–I–N Junction Arrays. Figure 1(c) shows the typical current–voltage characteristic curves for Si radial *p-i-n* wire array structures under dark and AM 1.5G illumination, exhibiting rectifying behavior indicating the formation of radial *p-i-n* junctions. The effect of match-heads on the PV response is clearly demonstrated in the current density–voltage (*J*–*V*) characteristic curves of the Si radial *p-i-n* junction arrays with and without match-heads in Figure 1(d). The PV performance as assessed by PV measurements under AM 1.5G illumination condition show a 16% higher short circuit current density (J_{sc}) value measured from arrays with match-heads (40.0 mA/cm^2) compared to those without match-heads (34.4 mA/cm^2). The resulting PV efficiency (10.1%) of the Si radial *p-i-n* junction arrays with match-heads is enhanced by 23% compared to that (8.2%) of Si radial *p-i-n* junction arrays without match-heads in the present case. There was no significant change for the open circuit voltage (V_{oc}) of 0.46 V and the fill factor (FF) of 0.52 of the Si radial *p-i-n* junction arrays with match-heads compared to the V_{oc} of 0.45 V and the FF of 0.51 of those without match-heads. We anticipate that further optimization of contact design and surface passivation could result in significantly increased absolute PV efficiency values.

Assessment of EQE and Absorption Enhancements by Experiment and Simulation. The enhancement of J_{sc}, as shown in Figure 1(d), is the main factor in improving the PV efficiency of Si radial *p-i-n* junction arrays with match-heads. To elucidate the origin of this enhancement of the J_{sc} for the match-heads we evaluated the arrays by wavelength-dependent EQE measurements and FDTD calculations of optical absorption. Figure 2(a) shows the measured EQE and calculated optical absorptance results of Si radial *p-i-n* junction arrays with and without match-heads. Both the EQE and optical

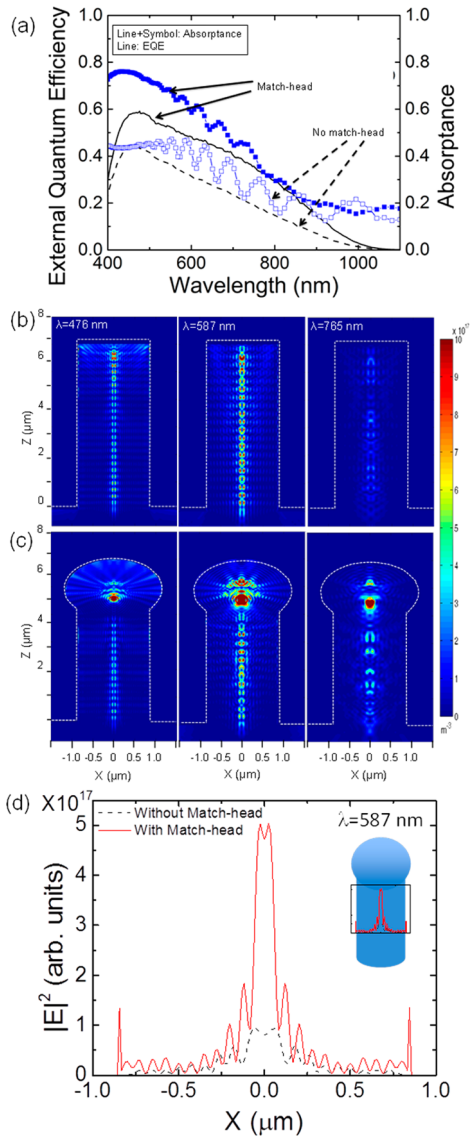

Figure 2. (a) The measured external quantum efficiency (lines) and the calculated absorptance (symbol+line) of Si radial *p-i-n* junction arrays with and without match-heads. The calculated monochromatic absorption profile cross sections through Si wires at the wavelengths 476, 587, and 765 nm (from left to right, respectively) without and with match-heads. Electric field intensity is illustrated by the color bar with red indicating stronger field intensity. (c) Radial distribution of calculated light intensity through the wire cross section with (solid line) and without (dashed line) match-heads at the wavelength of 587 nm at a distance of 3 μm from the tip of a 7 μm-long nanowire.

absorptance are enhanced up to 40% over all wavelengths for match-head structures. The oscillations with wavelength in the calculated optical absorptance originate from interference of the incident light in the arrays. The absence of such oscillations in the experimentally measured EQE is attributed to slight variation in the surface morphology, size or positions of NWs in the arrays. The decreased blue spectral response at wavelengths shorter than 450 nm in nanostructured Si solar cells has been attributed to both surface recombination due to absorption at shallow depths (less than 390 nm in Si) and high Auger recombination due to heavily doped emitter region formed by diffusion and annealing process.[25,26] The overall spectral shapes of the wavelength-dependent EQE and of the calculated optical absorptance curves in Figure 2(a) are not remarkably changed by the presence of the match-heads. This similarity of spectral shapes is consistent with the origin of the enhancements for both the light absorption and the EQE being due to a strengthening of the existing absorption mechanism with match-heads, as will be discussed in detail below.

Visualization of the light absorption spatial profile along the length of the wires at specific wavelengths provides additional insight in understanding the wavelength-dependent EQE curves. Figure 2(b) and (c) show truncated spatial cross sectional cuts of the calculated light absorptance of a single Si wire in arrays without and with spherical match-heads at the wavelengths of 476, 587, and 765 nm. The sizes and spacings of the wires for the calculation of Figure 2(b) and (c) are the same as those of the wires for the EQE and absorptance results of Figure 2(a). The absorbed light is seen to be guided to the center of each wire along the longitudinal axis both with and without the match-heads. This waveguiding effect is one of the principal mechanisms responsible for the enhancement of light absorption in NWs.[1] However, Figure 2(c) shows that there is an additional effect of the match-head, which acts as a light concentrator, thus providing a further significant enhancement in light absorption. Since the focal point for a specific wavelength changes along the length of the wire, this light concentrating effect works over a wide range of wavelengths and does not lead to a single localized hot spot. To illustrate the significance of the match-head light absorbing enhancement more quantitatively, the relative radial intensity profiles of light across a cross-sectional center of the wire at 3 μm from the top of a 7 μm long wire is shown in Figure 2(d) with and without a match-head for 587 nm light. The electric field intensity of the 587 nm-light in the match-head Si structure is remarkably greater than that of the Si wires without a match-head, thus resulting in the substantial enhancements observed in Figure 2(a).

The results presented in Figure 2 demonstrate that these match-heads act as a built-in, novel type of microscale light concentrator for PV devices. Traditionally photon management systems for concentrating sunlight have been categorized into two types: (1) solar tracking systems composed of lenses and curved mirrors at the macroscale for concentrating large amounts of sun light and (2) luminescent solar concentrators consisting of fluorescent pores such as dyes and quantum dots in transparent waveguides for collecting reemitted light and concentrating it on the PV cell at the end of a waveguide.[27,28] In contrast to both these types of solar concentration systems, which require additional processing to fabricate the concentrator systems, the match-head is

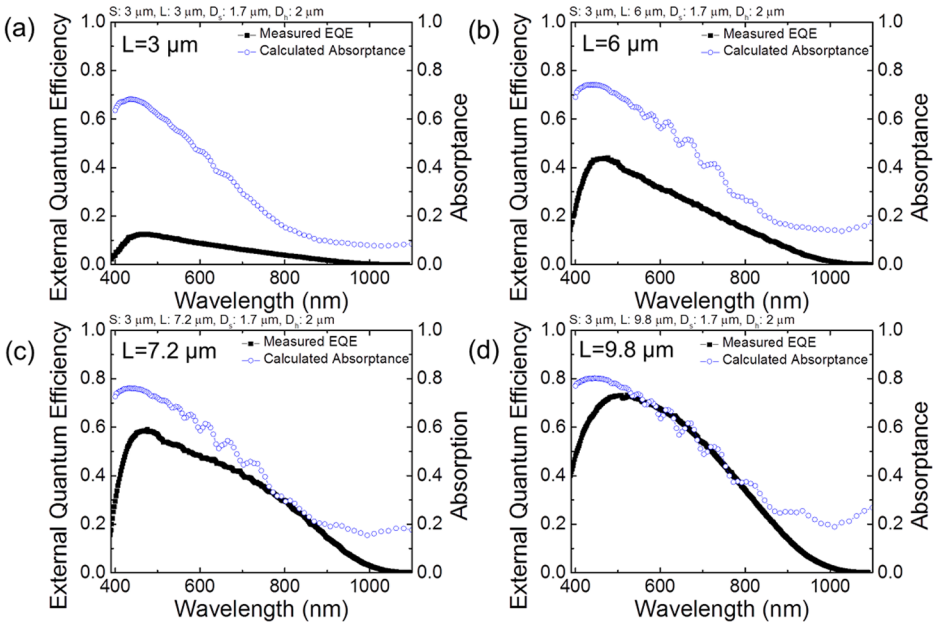

Figure 3. Length-dependent measured EQE and calculated absorptance of match-heads-Si wire arrays with fixed spacing (3 μm) and diameters (1.7 μm) of stem and (2.0 μm) of match-head for wire lengths: (a) 3 μm, (b) 6 μm, (c) 7.2 μm, and (d) 9.8 μm.

naturally formed and controlled with growth parameters during the radial epitaxy of our *p-i-n* junction wires without further processing. Additionally various shapes of match-heads such as hemisphere and pyramids might be employed to further optimize the light concentration effect.[29]

Assessment of Carrier Collection Efficiency Enhancement in Experiment and Simulation. For a more complete understanding of the enhanced PV characteristics in our structures, we studied the EQE and optical absorptance as a function of wavelength to infer additional information about the enhanced carrier collection efficiencies for different wire geometries. Figure 3(a)−(d) show double-axis plots of the wire-length-dependent EQE and calculated optical absorptance. An apparent trend is that the EQE values approach the calculated optical absorptance as the length of the Si wires increases. This approach indicates that the IQE is enhanced with increasing length of the Si wires. Furthermore, the wavelength-dependent EQE curves overlap the calculated optical absorptance curves in the case of Si radial *p-i-n* junction arrays longer than 7.2 μm. We note that the direct determination of IQE was not available in the present study since the optical absorptance was only determined by FDTD calculations. For 7.2 μm-long Si radial *p-i-n* junction arrays the EQE values reach the calculated absorptance around 800 nm, and at 9.8 μm length the EQE overlaps the calculated optical absorptance curve over wavelengths ranging from 570 to 800 nm. This overlap of EQE and calculated optical absorptance implies a high IQE, approaching ~100%.

The increase in IQE enhancement with NW length, interpreted from the approach of the EQE curve to the calculated optical absorptance shown in Figure 3(a) and (d), between 3 and 9.8 μm-long Si radial *p-i-n* junction arrays, gives rise to the question of why the shorter Si radial *p-i-n* junction arrays do not fully utilize the efficient radial carrier collection. Since the collection efficiency of photogenerated carriers depends on the carrier loss mechanism, we must consider what aspects of the spatial distribution of photogenerated carriers may be affecting the carrier collection for the shorter wire arrays. Figure 4(a) shows the optical absorption spatial profiles of 3 and 7.2 μm-long Si radial *p-i-n* junction arrays in wires with the same match-head and stem diameter for the wavelengths of 476, 587, and 785 nm. While both 3 and 7.2 μm-long cases show the light concentration effect at the center of the wire, the match-head becomes a larger fraction of the absorbing volume as the length of the stem decreases for shorter wires. As shown in Figure 4(a) the light absorption intensity in the match-head extends more to the surface than in the stem. Since absorbed light in the regions closer to surface has a higher chance of recombination through both surface channels and the Auger process dominant in the outmost *n*-type Si shell with the estimated doping concentration of $1.3 \times 10^{19}/cm^3$, the overall collection efficiency decreases for shorter wires. Figure 4(b) and (c) display an electric field intensity cross section profile of absorbed light in the match-head and in the "stem". In the stem light absorption mainly occurs in the center region along the longitudinal axis due to the light concentrating effect of the match-head, whereas in the match-head the electric field intensity profile extends closer to the surface along radial direction (Figure 4(c)). The volume fractions of the 1.7 μm-diameter match-head for the 3 μm-long and 7.2 μm-long Si wires

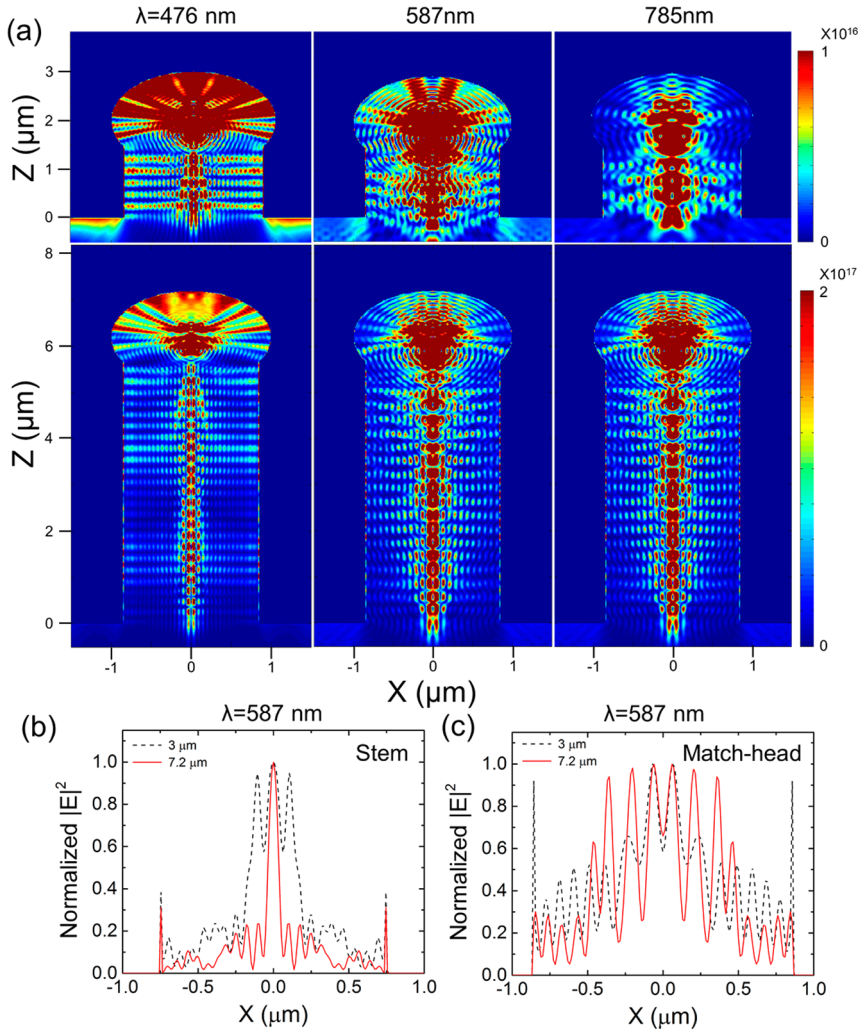

Figure 4. (a) The optical absorption profiles illustrated in color of single Si radial *p-i-n* junction structures in arrays with two different lengths of 3 μm (upper panels) and 7.2 μm (lower panels) at the wavelengths of 476, 587, 785 nm (left to right). Note change in color bar scale for field intensity. The normalized electric field intensity profiles across the stem at 1 μm from wire base (b) and across the center of the match-head (c) for the lengths of 3 and 7.2 μm is shown at the wavelength 587 nm.

compared to the total volume are about 60 and 26%, respectively. Thus, a greater contribution of photogenerated carrier recombination nearer the surface in the match-heads compared to the stems will show a relative decrease with increasing length of the wires, leading to the observed length-dependent improvement in EQE with wire length shown in Figure 3.

Influence of Array Geometry on PV Performance. A complete picture of the design rules for high-performance PV device arrays needs to account for the overall array geometry, in addition to the length of individual array elements. Thus, we studied the combined effects of wire length, diameter, and spacing for Si radial *p-i-n* junction arrays with match-heads to investigate optimal designs for higher J_{sc} (higher EQE). Figure 5(a)−(f) show examples of the measured EQE and corresponding calculated absorptance for Si radial *p-i-n* junction arrays while varying the parameters of wire *length* at fixed diameter and spacing (a,b), wire *diameter* at fixed spacing and length (c,d), and wire *spacing* at fixed diameter and length (e,f). Figure 5(a) and (b) show the length-dependent results for arrays with a fixed center to center spacing of 3 μm and fixed diameters of 1.8 μm (stem) and 2.1 μm (match-head). As the length of the Si wires increases an increasing amount of the available incident light is absorbed and both the EQE values and the optical absorption increase. At sufficient lengths of ~10 μm this increase saturates as the light absorption in the wires becomes more complete. We note that the enhancement of EQE is remarkably stronger compared to that of the optical absorptance with increase in the NW length. For example, the EQE at 600 nm increases from 16% for 3 μm-long Si wires to 67% (a factor of 4) for 9.8 μm-long Si wires at a fixed 1.8 μm diameter and 3 μm spacing. In contrast, the optical absorptance at 600 nm is only enhanced from 45 to 76% (a factor of 1.7) for the same case.

Similar enhancement behavior in array performance is observed for the Si radial *p-i-n* junction arrays at the same spacing (3 μm) with increasing wire diameter.

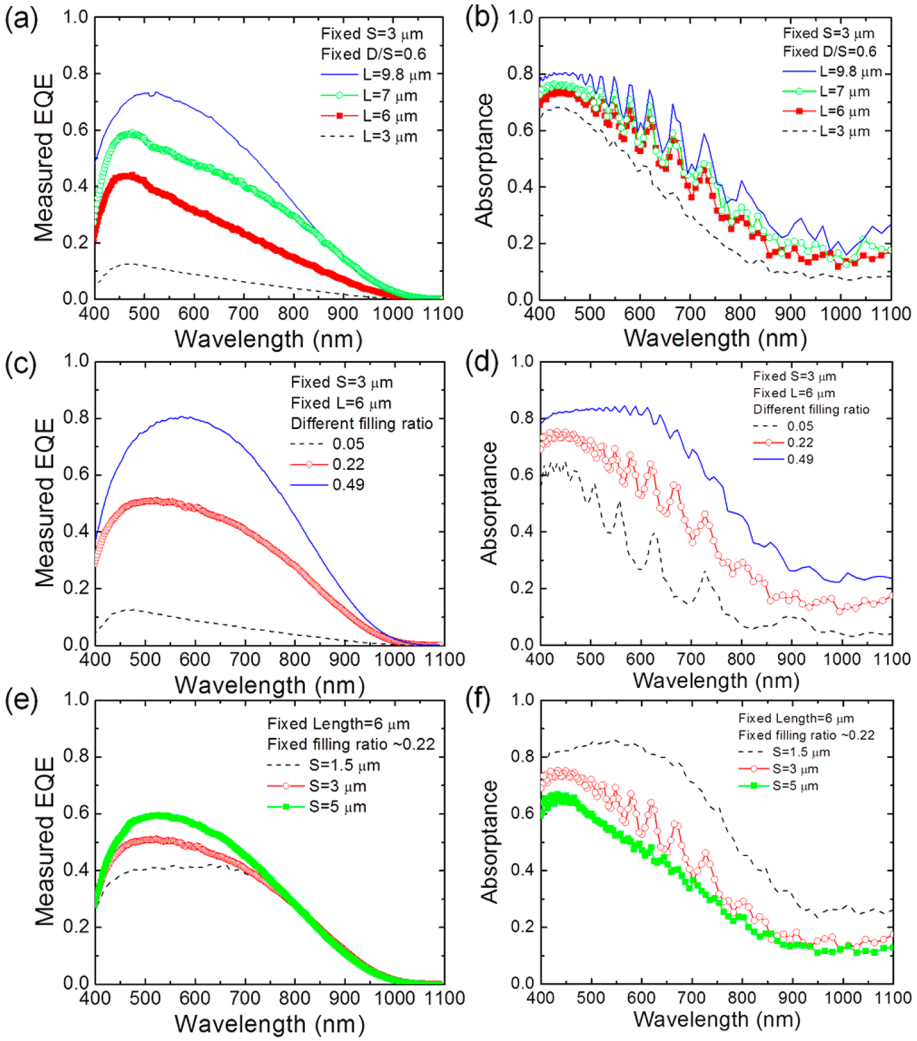

Figure 5. Parametric study of the measured EQE and calculated absorptance values for radial Si *p-i-n* wire arrays as a function of (a, b) wire lengths at fixed wire diameter and spacing, (c, d) filling ratios as controlled by the wire diameter for fixed wire spacing and length, and (e, f) spacing between wires for a fixed length and constant filling ratio of 0.22.

The change in diameter at fixed spacing is expressed by the filling ratio, the fraction of available volume filled by Si in a given layer thickness and denoted here by the ratio of projection area of wire to that of a unit cell defined by the wire spacing. Figure 5(c) and (d) show the diameter-dependent results for the fixed length of 6 μm and fixed spacing of 3 μm, with the filling ratio varied from 0.05 to 0.49. The increase in the stem diameter at fixed spacing increases the filling ratio, which is observed to enhance both the EQE and the optical absorptance. The enhancement of optical absorption in longer and thicker Si wires can be explained by the increase in total absorption volume. Similar to that for the NW length dependence, the enhancement of EQE is remarkably stronger compared to that of the optical absorptance with increase in filling ratio. This difference implies that in addition to the increased light absorption due to a greater filling ratio, there is an extra increase in carrier collection efficiency, as detected by the larger increase in EQE. Thus, the increase in EQE with diameter can be understood as due to a decrease in recombination loss at the wire surfaces.

To further explore this understanding of an enhanced efficiency in carrier collection at larger wire diameters due to reduced surface recombination, we varied the wire spacings at a fixed filling ratio. The wire spacing has been a common parameter in optical absorption studies to tune the absorption properties of ordered Si wire arrays,[6−9,30] but it has not commonly been coupled to consideration of the carrier collection efficiency. Here, in maintaining a fixed filling ratio the wire diameter increases as the wire spacing increases. Thus, we are able to better examine the influence on carrier collection efficiency without the large change in light absorption due to a changing filling ratio. Figure 5(e) and (f) show the spacing-dependent EQE results and calculated absorptance of Si radial *p-i-n* junction arrays with a fixed length of 6 μm and the fixed filling ratio of 0.22. In this parameter region the spacing-dependent EQE results and optical

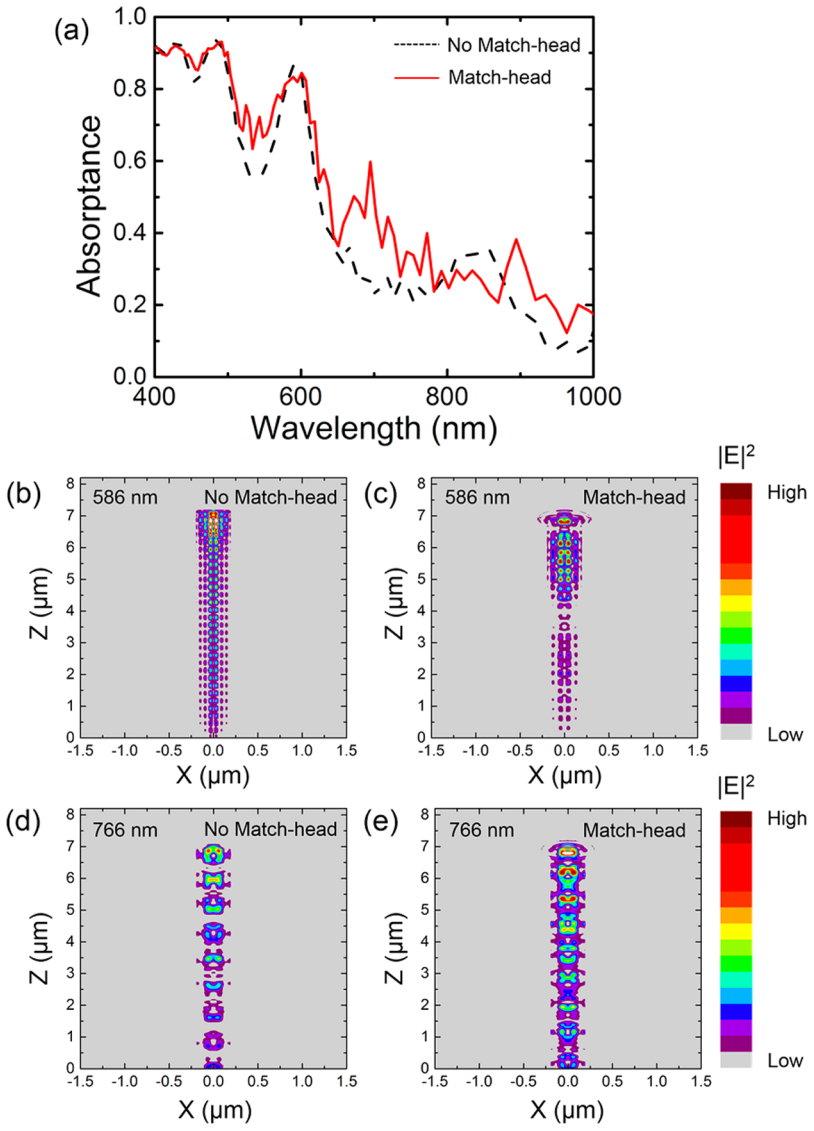

Figure 6. (a) The wavelength-dependent calculated absorptance curves of Si wires with and without match-heads. The stem diameter, the length, and the spacing are 400 nm, 7.2, and 3 μm, respectively. The match-head diameter is 600 nm. (b)−(e) The truncated view of the calculated monochromatic absorption profile cross sections through single Si wires at the wavelengths 586 and 766 nm without and with match-heads. Electric field intensity is illustrated by the color bar with red indicating stronger field intensity.

absorptance exhibit an opposite dependence, in contrast to the length and the diameter (filling ratio) dependent trends. The origin of the enhanced optical absorption in this narrower spacing regime has been attributed to enhanced light scattering at the submicrometer scale. However, the decrease in EQE value here, even as the optical absorption is enhanced at very small spacings, shows that the PV performance as represented by EQE is not governed primarily by optical absorption in this regime. Rather the results support the above interpretation that the smaller diameter at smaller spacings to maintain a fixed filling ratio leads to a decrease in carrier collection efficiency due to an increase in surface recombination. In the present case the larger spacing of 5 μm is seen to be near optimum for a filling ratio of 0.22 and corresponds to a wire diameter of 3 μm. Thus, there is a trade-off in the need to maintain a dense array of small diameter wires to optimize optical absorption and the need to maintain large enough diameter wires to achieve efficient carrier collection for optimum PV performance.

Effect of Match-Head in Submicrometer Scale. The main effect of match-head on PV performances is enhanced light absorption due to light concentration resulted from geometrical shape of top regions of wires. In addition to the systematic studies described and discussed above in the micrometer scale the effect of match-head on light absorption characteristics of Si wires of which diameters are submicrometer scale was investigated by FDTD calculation. Figure 6(a)−(e) show the wavelength-dependent optical absorptance curves and cross-sectional monochromatic optical absorption

profiles of Si wires with and without match-head. The stem diameter, the length, and the spacing were 400 nm, 7.2, and 3 μm, respectively. The match-head diameter was 600 nm. According to Figure 6(a) the optical absorptance of the match-head case is enhanced by about 10%. A noticeable feature of optical absorptance in submicrometer scale is that the spectral shapes of the calculated optical absorptance curves are different along match-head formation. Match-head in submicrometer scale induces enhanced absorption in longer wavelengths. On the other hand, the spectral shapes of the calculated optical absorptance curve of Si wires in microscale (Figure 2(a)) were almost identical regardless of match-head formation. Figure 6(b)−(e) visualize the change of light absorption spatial profiles of Si nanowires with and without match-head clearly. The truncated spatial cross sectional cuts of the calculated light absorptance of a single Si nanowire in arrays without and with spherical match-heads at the wavelengths of 586 and 766 nm. For both Si nanowires with and without match-heads waveguiding effect is seen in the calculated absorption profiles. Additionally match-head induces light concentration effect at 766 nm. The enhanced light absorption is consistent with Figure 6(a). The results presented in Figure 6 indicate that the advantages of match-head formation in microscale can be obtained in submicrometer scale. The extended calculation results of different diameters of 200 and 600 nm are summarized in the Supporting Information.

CONCLUSION

In summary, an integrated study of the measured EQE and FDTD calculated optical absorption has been carried out for a new Si radial *p-i-n* junction wire array architecture containing match-heads at the wire tips. The match heads have a larger diameter than the wires and act as miniature optical focusing elements. They are demonstrated to enhance the PV efficiency by 23% (8.2 to 10.1%). This morphological control of Si radial *p-i-n* junction array geometry has provided a means to study and better understand the interplay between optical absorption and material structuring in carrier collection efficiency, thus helping to elucidate nanowire array design rules for photovoltaic applications. Our results indicate that the match-head structure enhances both optical absorptance and external quantum efficiencies by 30 to 40% compared to cylindrical structures without match-heads. The visualization of the spatial optical absorption profiles shows how the match-heads act as light concentrators, directing a higher intensity of light into the central region of the Si wire over the range of visible wavelengths. This light concentrating effect by match-heads, which are formed as a consequence of the radial *p-i-n* epitaxial growth process, provides a novel pathway to achieve photon management without additional device architecture processing requirements. The strategy of morphological design for enhancing photovoltaic performance can also be utilized in other semiconductors such as Ge, GaN, and GaP since the formation of match-heads is a natural consequence of surface energy minimization in three-dimensional crystal growth.[31−33] Furthermore, the strategy of three-dimensional crystal growth with nanoscale control of growth can be generally applicable to nano- and microstructures. In the present studies we have used e-beam patterning and top down etching to fabricate the arrays for radial growth in order to investigate a wide range of precisely controlled array geometries. However, the epitaxial growth mechanism employed here of enhanced facet formation during B-doped Si radial epitaxy could be applied to more scalable array fabrication approaches for practical application. In addition, our comprehensive study of quantum efficiency and optical absorption of match-head-Si radial *p-i-n* junction arrays demonstrates that to optimize PV performance through the geometric wire array parameters, one must account for the design trade-off between maintaining sufficiently large wire diameters to minimize surface recombination loss while maintaining close wire spacings with large filling ratios to maximize light absorption. These results indicate that carrier collection in radial *p-i-n* junction PV wire devices can be highly efficient, and demonstrates how management of the spatial distribution of photogenerated carriers in wires provides an important tool to optimize the carrier collection in radial *p-n* junction arrays for improved photovoltaic performance.

METHODS

Epitaxial Growth of Si Radial *p-i-n* Junction Arrays. Silicon radial *p-i-n* junction wire arrays were prepared by top-down fabrication of *p*-type Si wire cores, followed by the subsequent epitaxial growth of Si radial shells in the sequence of *p*-type, intrinsic, and *n*-type layers. The Si radial *p-i-n* junction arrays were grown by Si radial epitaxy *via* low-pressure chemical vapor deposition (CVD) in a cold wall stainless steel reactor. Silane (SiH_4) diluted with a 50% hydrogen concentration was the growth precursor with phosphine (PH_3, 5000 ppm) and diborane (B_2H_6, 100 ppm) diluted in hydrogen as the dopants precursors. The growth temperature and the partial pressure of SiH_4 were 810 °C and 7.5 mTorr, respectively. For doped Si growth, the dopant precursor to SiH_4 precursor gas ratios were fixed at 3.3×10^{-6} for B_2H_6 and 6×10^{-5} for PH_3. The resulting dopant concentrations determined by 4-probe measurements on planar epitaxial reference layers were 3.3×10^{18}/cm^3 for *p*-type Si(B) (identical to the p-type Si [111] substrate used to form the NW cores) and 1.3×10^{19}/cm^3 for *n*-type Si(P). The growth rates of intrinsic Si, *p*-type Si(B), and *n*-type Si(P) radial shells on the Si NWs of 500 nm diameter were 30, 20, and 8 nm/min, respectively.

Conflict of Interest: The authors declare no competing financial interest.

Acknowledgment. This work was performed in part at CINT, a U.S. Department of Energy, Office of Basic Energy Sciences

User Facility at Los Alamos National Laboratory (Contract DE-AC52-06NA25396) and Sandia National Laboratories (Contract DE-AC04-94AL85000), and funded in part by the Laboratory Directed Research and Development Program at LANL and the DOE Office of Energy Efficiency and Renewable Energy, Solar Energy Program (EB2101010), a director's postdoctoral fellowship for B.-M.N. at Los Alamos National Laboratory. S.A.D. acknowledges support from the US National Science Foundation (CBET-1236155 and ECCS-1351980).

Supporting Information Available: Preparation of core silicon nanowires, device fabrication for external quantum efficiency/photovoltaic measurements, and finite difference time domain calculations are described. The Supporting Information is available free of charge on the ACS Publications website at DOI: 10.1021/acsnano.5b00500.

REFERENCES AND NOTES

1. Narasimhan, V.; Cui, Y. Nanostructures for Photon Management in Solar Cells. *Nanophotonics* **2013**, *2*, 187–210.
2. Zhu, J.; Yu, Z.; Burkhard, G. F.; Hsu, C.-M.; Connor, S. T.; Xu, Y.; Wang, Q.; McGehee, M.; Fan, S.; Cui, Y. Optical Absorption Enhancement in Amorphous Silicon Nanowrie and Nanocone Arrays. *Nano Lett.* **2009**, *9*, 279–282.
3. Bao, H.; Ruan, X. Optical Absorption Enhancement in Disordered Vertical Silicon Nanowire Arrays for Photovoltaic Applications. *Opt. Lett.* **2010**, *35*, 3378–3381.
4. Tsai, M.-A.; Tseng, P.-C.; Chen, H.-C.; Kuo, H.-C.; Yu, P. Enhanced Conversion Efficiency of a Crystalline Silicon Solar Cell with Frustum Nanorod Arrays. *Opt. Express* **2010**, *19*, A28–A34.
5. Kim, S.-K.; Day, R. W.; Cahoon, J. F.; Kempa, T.; Song, K.-D.; Park, H.-G.; Lieber, C. M. Tuning Light Absorption in Core/Shell Silicon Nanowire Photovoltaic Devices through Morphological Design. *Nano Lett.* **2012**, *12*, 4971–4976.
6. Hu, L.; Chen, G. Analysis of Optical Absorption in Silicon Nanowire Arrays for Photovoltaic Applications. *Nano Lett.* **2007**, *7*, 3249–3252.
7. Lin, C.; Povinelli, M. L. Optical Absorption Enhancement in Silicon Nanowire Arrays with a Large Lattice Constant for Photovoltaic Applications. *Opt. Express* **2009**, *17*, 19371–19381.
8. Alaeian, H.; Atre, A. C.; Dionne, J. A. Optimized Light Absorption in Si Wire Arrays Solar Cells. *J. Opt.* **2012**, *14*, 024006.
9. Li, J.; Yu, H.; Li, Y. Solar Energy Harnessing in Hexagonally Arranged Si Nanowire Arrays and Effects of Arrays Symmetry on Optical Characteristics. *Nanotechnology* **2012**, *23*, 194010.
10. Zhan, Y.; Li, X.; Li, Y. Numerical Simulation of Light-Trapping and Photoelectric Conversion in Single Nanowire Silicon Solar Cells. *IEEE J. Sel. Top. Quantum Electron.* **2013**, *19*, 4000208.
11. Yoo, J.; Dayeh, S. A.; Tang, W.; Picraux, S. T. Epitaxial Growth of Radial Si P-I-N Junctions for Photovoltaic Applications. *Appl. Phys. Lett.* **2013**, *102*, 093113.
12. Um, H.-D.; Park, K.-T.; Jung, J.-Y.; Li, X.; Zhou, K.; Lee, S.-W.; Lee, J.-H. Incorporation of a Self-Aligned Selective Emitter to Realize Highly Efficient (12.8%) Si Nanowire Solar Cells. *Nanoscale* **2014**, *6*, 5193–5199.
13. Lu, Y.; Lal, A. High-Efficiency Ordered Silicon Nano-Conical-Frustrum Array Solar Cells by Self-Powered Parallel Electron Lithography. *Nano Lett.* **2010**, *10*, 4651–4656.
14. Oh, J.; Yuan, H.-C.; Branz, H. M. An 18.2%-Efficient Black-Silicon Solar Cell Achieved through Control of Carrier Recombination in Nanostructures. *Nat. Nanotechnol.* **2012**, *7*, 743–748.
15. Zhang, Y.; Cui, W.; Zhu, Y.; Zu, F.; Liao, L.; Lee, S.-T.; Sun, B. High Efficiency Hybrid PEDOT:PSS/Nanostructured Silicon Schottky Junction Solar Cells by Doping-Free Rear Contact. *Energy Environ. Sci.* **2015**, *8*, 297–302.
16. Kayes, B. M.; Atwater, H. A.; Lewis, N. S. Comparison of the Device Physics Principles of Planar and Radial P-N Junction Nanorod Solar Cells. *J. Appl. Phys.* **2005**, *97*, 114302.
17. Kelzenberg, M. D.; Boettcher, S. W.; Petykiewicz, J. A.; Turner-Evans, D. B.; Putnam, M. C.; Warren, E. L.; Spurgeon, J. M.; Briggs, R. M.; Lewis, N. S.; Atwater, H. A. Enhanced Absorption and Carrier Collection in Si Wire Arrays for Photovoltaic Applications. *Nat. Mater.* **2010**, *9*, 239–244.
18. Mohite, A. D.; Perea, D. E.; Singh, S.; Dayeh, S. A.; Campbell, I. H.; Picraux, S. T.; Htoon, H. Highly Efficient Charge Separation and Collection across *In Situ* Doped Axial VLS-Grown Si Nanowire P-N Junctions. *Nano Lett.* **2012**, *12*, 1965–1971.
19. Putnam, M. C.; Turner-Evans, D. B.; Kelzenberg, M. D.; Boettcher, S. W.; Lewis, N. S.; Atwater, H. A. 10 Micrometer Minority-Carrier Diffusion Lengths in Si Wires Synthesized by Cu-Catalyzed Vapor-Liquid-Solid Growth. *Appl. Phys. Lett.* **2009**, *95*, 163116.
20. Kendrick, C. E.; Eichfeld, S. M.; Ke, Y.; Weng, X.; Wang, X.; Mayer, T. S.; Redwing, J. M. Epitaxial Regrowth of Silicon for the Fabrication of Radial Junction Nanowire Solar Cells. *Proc. SPIE* **2010**, *7768*, 77680I.
21. Tvingstedt, K.; Zilio, S. D.; Inganäs, O.; Tormen, M. Trapping Light with Micro Lenses in Thin Film Organic Photovoltaic Cells. *Opt. Express* **2008**, *16*, 21608–21615.
22. Yoo, J.; Dayeh, S. A.; Bartelt, N. C.; Tang, W.; Findikoglu, A. T.; Picraux, S. T. Size-Dependent Silicon Epitaxy at Mesoscale Dimensions. *Nano Lett.* **2014**, *14*, 6121–6126.
23. Eaglesham, D. J.; White, A. E.; Feldman, L. C.; Moriya, N.; Jacobson, D. C. Equilibrium Shape of Si. *Phys. Rev. Lett.* **1993**, *70*, 1643–1646.
24. Cho, B.; Bareño, J.; Foo, Y. L.; Hong, S.; Spila, T.; Petrov, I.; Greene, J. E. Phosphorous Incorporation during Si(001):P Gas-Source Molecular Beam Epitaxy: Effects on Growth Kinetics and Surface Morphology. *J. Appl. Phys.* **2008**, *103*, 123530.
25. Green, M. A. *Solar Cells: Operating Principles, Technology, and System Applications*; Prentice Hall: Upper Saddle River, NJ, 1982.
26. Zhai, X.; Wu, S.; Shang, A.; Li, X. Limiting Efficiency Calculation of Silicon Single-Nanowire Solar Cells with Considering Auger Recombination. *Appl. Phys. Lett.* **2015**, *106*, 063904.
27. Weber, W. H.; Lambe, J. Luminescent Greenhouse Collector for Solar Radiation. *Appl. Opt.* **1976**, *15*, 2299–2300.
28. Currie, M. J.; Mapel, J. K.; Heidel, T. D.; Goffri, S.; Baldo, M. A. High-Efficiency Organic Solar Concentrators for Photovoltaics. *Science* **2008**, *321*, 226–228.
29. Zhu, J.; Hsu, C.-M.; Yu, Z.; Fan, S.; Cui, Y. Nanodome Solar Cells with Efficient Light Management and Self-Cleaning. *Nano Lett.* **2010**, *10*, 1979–1984.
30. Sturmberg, B.; Dossou, K. B.; Botten, L. C.; Asatryan, A. A.; Poulton, C. G.; Martijin de Sterke, C.; McPhedran, R. C. Modal Analysis of Enhanced Absorption in Silicon Nanowire Arrays. *Opt. Express* **2011**, *19*, A1067–A1081.
31. ElAhl, A. M. S.; He, M.; Zhou, P.; Harris, G. L.; Salamanca-Riba, L.; Felt, F.; Shaw, H. C.; Sharma, A.; Jah, M.; Lakins, D.; *et al.* Systematic Study of Effects of Growth Conditions on the (Nano-, Meso-, Micro)size and (One-, Two-, Three-Dimensional) Shape of GaN Single Crystals Grown by a Direct Reaction of Ga with Ammonia. *J. Appl. Phys.* **2003**, *94*, 7749–7756.
32. Falub, C. V.; von Känel, H.; Isa, F.; Bergamaschini, R.; Marzegalli, A.; Chrastina, D.; Isella, G.; Müller, E.; Niedermann, P.; Miglio, L. Scaling Hetero-Epitaxy from Layers to Three-Dimensional Crystals. *Science* **2012**, *335*, 1330–1334.
33. Strandwitz, N.; Turner-Evans, D. B.; Tamboli, A. C.; Chen, C. T.; Atwater, H. A.; Lewis, N. S. Photoelectrochemical Behavior of Planar and Microwire-Array Si-GaP Electrodes. *Adv. Energy Mater.* **2012**, *2*, 1109–1116.